Peer reviewed version

Link to published version (if available):
10.1016/j.scriptamat.2015.10.033

Link to publication record in Explore Bristol Research
PDF-document

University of Bristol - Explore Bristol Research
General rights

Three-Dimensional Displacement Mapping of Diffused Pt Thermal Barrier Coatings via Synchrotron X-ray Computed Tomography and Digital Volume Correlation

D. Khoshkhou[a], M. Mostafavi[b,1], C. Reinhard[c], M. P. Taylor[a], D. S. Rickerby[d], I. M. Edmonds[d], H. E. Evans[a], T.J. Marrow[b], B.J. Connolly[a,2]

[a] School of Metallurgy & Materials, University of Birmingham, Birmingham, B15 2TT, UK
[b] Department of Materials and Oxford Martin School, The University of Oxford, Oxford, OX1 3PH, UK
[c] I12 JEEP Beamline, Diamond Light Source, Harwell Science & Innovation Campus, Didcot OX11 0DE, UK
[d] Rolls-Royce plc, PO Box 31, Derby DE24 8BJ, UK.

A progressive study of the three-dimensional deformation field within a γ/γ' thermal barrier coating following cyclic oxidation at 1200°C is presented, observed using synchrotron X-ray micro-computed tomography and analysed by Digital Volume Correlation. Oxide thickening and bondcoat creep displacements are quantified as a function of exposure time at temperature. Linear gradients of these displacements are measured both in-plane and normal to the oxide layer. The first thermal cycle shows the most displacement changes; destructive sectioning confirms the DVC-calculated displacement magnitudes.

Keywords: Thermal barrier coating, three-dimensional tomography, synchrotron radiation, cyclic oxidation, digital volume correlation

Thermal Barrier Coatings (TBCs) applied to gas turbine components in both aerospace and land-based applications allow increased turbine inlet temperatures and fuel efficiency. Full exploitation of TBCs and prediction of the remaining useful life is limited by an incomplete understanding of TBC failure mechanisms. Typical current-generation diffusion coating systems consist of an yttria partially-stabilised zirconia topcoat, an alumina thermally grown oxide (TGO) and an aluminium-rich metallic bondcoat. At operating temperatures, oxidation-induced growth stresses and mismatches in thermal expansions of these constituents generate residual strains [1], which may eventually lead to spallation of the thermally protective topcoat and/or the TGO.

The most commonly used technique, to date, for monitoring the evolution of TGO residual stresses is photo-luminescence piezospectroscopy (PLPS) [2]. Although PLPS allows imaging of production and in-service TBCs, the key limitations of the technique are an inability to resolve out-of-plane strains and a limited spatial resolution (on the order of 20-50 μm) due to beam scattering within the topcoat. Other approaches utilising synchrotron X-ray diffraction (XRD) [3–5] have recently been used to measure elastic strains within TBC layers. The through thickness averaging characteristic of this 2-dimensional (2-D) method however, does not allow identification of local out-of-plane strains. Other attempts to measure local strains in TBCs have involved the use of neutron [6] diffraction that restricts mapping in 3-dimensional (3-D) space. The importance of out-of-plane strains and total deformation, either neglected or only partially explored by the aforementioned techniques has been underscored by failure prediction models [7]. One approach to obtaining full-field 3-D displacement and strain fields, as pursued in this contribution, is to combine a 3-D volumetric imaging technique such as X-ray computed tomography [8] or laminography [9] with a high precision measurement technique such as digital image correlation [10].

Digital Image and Digital Volume Correlation (DIC and DVC, respectively) are 2-D and 3-D image analysis techniques that map relative displacements across a time-dependent sequence of images. DIC and DVC divide each data set (i.e., images) into smaller subsets, commonly known as interrogation windows. By maximising the correlation coefficient for each interrogation window between successive images, the relative displacement and deformation of each interrogation window is calculated. The computed displacement field can be used to derive total strain fields, from which the position of strain-influencing features such as cracks [11], for instance, may be inferred. It is noteworthy that the inputs are digital images and the technique is consequently independent of the image acquisition technique and hence length scale [12]. Additionally, displacements can be computed beyond the resolution of the imaging technique (i.e., sub-pixel and sub-voxel, respectively) [13]. DIC techniques have previously been used to characterise the mechanical properties of TBCs [14] but were limited to 2-D surface imaging and lacked the capability of probing internal volumes.

---

[1] Present address: Department of Mechanical Engineering, University of Bristol, Queen's Building, University Walk, Bristol, BS8 1TR
[2] Corresponding Author: b.j.connolly@bham.ac.uk

In the present work, DVC was coupled with high resolution synchrotron X-ray absorption computed micro-tomography to study, in a near in-situ fashion, the progressive development of the oxidation induced displacement field within a TBC system undergoing cyclic oxidation. The TBC system examined was the second-generation single crystal nickel superalloy CMSX-4, with a diffused platinum γ/γ' bondcoat [15]. The ceramic topcoat was a 135 µm thick electron beam-physical vapour deposited (EB-PVD) yttria partially stabilised zirconia (7-YPSZ) coating. Cylindrical specimens, 500 µm in diameter, were prepared from turbine components. These samples were thermally exposed in a horizontal tube furnace in laboratory air for twenty-hour cycles at 1200°C from the as-received state. Following removal from the furnace at the end of each exposure period, the samples were allowed twenty minutes to reach the room temperature of 21°C (without forced cooling) before imaging via synchrotron X-ray micro-tomography. Following completion of each scan, the samples were returned to the furnace for the next twenty-hour exposure period. This experimental schema allowed a near in-situ imaging of the same specimen as a function of time at temperature.

The synchrotron X-ray micro-tomography was carried out at the I12 Joint Engineering, Environmental and Processing (JEEP) beamline [16] at the Diamond Light Source (UK). A monochromatic beam of 53 keV was used in absorption contrast configuration, with a camera to sample distance of 300 mm which provided some phase contrast; the PCO 4000 camera with a field of view of 3.6×2.4 mm delivered a nominal pixel resolution of 0.9 µm. Samples were positioned such that the beam was approximately parallel to the planar interface of the TBC layers. The cylindrical specimen geometry allowed uniform beam penetration to minimise reconstruction artefacts. The tomography scans were over 180° with 0.06° steps between radiographs, with an exposure time of 3.0s per step. Back-filtered projection reconstruction was carried out using the in-house reconstruction algorithm at I12 [17]. Finally, the grey-scale distributions (down-sampled to 8 bit) of the reconstructed tomographs were normalised relative to the substrate bulk grey-level of the as-received condition, prior to image correlation analysis.

Reconstructed planar tomography sections (Fig. 1a and Fig. 1b) allowed direct observation of TBC microstructure evolution, at the same location within the sample, as a function of exposure time at temperature. The different TBC layers were discernible owing to the density-dominated differences in relative X-ray attenuation between the topcoat (3.960 cm^2/g), alumina TGO (0.276 cm^2/g), bondcoat (4.422 cm^2/g in the as-received state), the substrate (2.417 cm^2/g) and air (0.201 cm^2/g); all attenuations calculated at 53 keV using WinXCom [18]. Some regions of the TGO were observed in the as-received case while other regions of the TGO (measured at 0.3– 1.1 µm metallographically) fell below the detectable resolution limit at 0.9 µm voxel size. Within the bondcoat, entrapped alumina particles attributable to the grit-blasting process during coating manufacture (grit line) were also observed. The boundary between the γ' dominated lamellar regions of the bondcoat was clearly visible against the more strongly attenuating (i.e., darker) γ phase of the bondcoat.

Following 40 hours of exposure (two 20-hour periods) of the same specimen at 1200°C (Fig. 2b), thickening of the TGO was observed; in independent samples treated identically, the TGO thickness was measured between 2.6 and 4 µm. Bondcoat phase transformation was also observed, visible as an extension of the brighter bondcoat layer downward into the substrate. This change corresponds to an outward diffusion of Al and destabilisation of the Pt-rich γ' phase leading to the diffusion of Pt into the substrate.

DVC, implemented using the LaVision DaVis Strain Master 8.2.2 software was applied to cropped regions of the X-ray tomographs. The first time step compared the as-received sample to the 20-hour oxidation exposure (i.e., scan after one thermal cycle – Fig. 1c). The second timestep compared the 20 hours exposure to the 40 hours exposure, and the third time-step compared the 60-hour exposure to the 80-hour exposure (Fig. 1d). The DVC interrogation subsets were iteratively reduced from 128×128×128 voxels to 16×16×16 voxels over 3 iterations with a 50% subset overlap at each stage. Displacement vectors having correlation coefficients less than 50% were excluded. Rigid body translation and fine rotations of the output vector field that arose during sample exchange were corrected using an efficient algorithm [13], which was also used to obtain the displacement field in a coordinate system that was precisely aligned with the topcoat and TGO interface.

Representative planar slices through the obtained displacement fields were extracted from the vicinity of the topcoat and the TGO (Fig. 2). The maps show displacement vectors (indicated by arrows) overlaid on a contour map of displacement magnitude in the plane of the TGO (Fig. 2a) and out-of-plane of the TGO (Fig 2b). White patches on the map indicate regions that did not meet the 50% minimum correlation coefficient criterion. A likely cause of poor correlation within the lower portion of the topcoat is the fine nature and possible sintering of inter-columnar features, which presents an inherent difficulty in their observation via X-ray attenuation tomography at the current resolution; limited features are thus available for image correlation to operate on. In contrast, the columns are larger and well-defined in the upper regions of the topcoat, and hence continuous displacement contours are observed. The majority of the substrate exhibited poor correlation, due to the lack of traceable features in its structure. The in-plane

map (Fig 2a) reveals a horizontal gradient in the lateral displacements from the edges of the specimen to the plane centre. There is also a vertical gradient near the sample edges indicating greater lateral displacement within the topcoat competition zone as opposed to the near surface region. The out-of-plane map (Fig. 2b) suggests a near-uniform upward displacement of the topcoat bulk. The outer edges of the near-surface region within the topcoat appear to undergo greater out-of-plane displacements than the central near-surface region.

To quantify the variation in displacement in and around the TGO, displacement profiles were extracted from the X-Y plane of the TGO region (dashed lines in Fig. 2). Although the base of the topcoat did not correlate satisfactorily in all areas, a planar section of the DVC displacement field (7.2 µm thick), encompassing the TGO, provided sufficient displacement vectors to extract in-plane and out-of plane displacement values (~55% of the vectors in this section has correlation coefficients below 50% and were not included). The average displacement as a function of the radial position about the specimen cylindrical axis midpoint in the plane of the TGO was extracted and is presented in Fig. 3.

The in-plane displacements at the TGO (Fig. 3a) show the greatest total outward deformation (5-10µm, also confirmed metallographically as δ in Fig. 4b) over the first time step, increasing to the extremities of the specimen with an approximately constant dimensional change rate or strain of 3.3%. An additional outward displacement of up to 2-5 µm (average strain of 0.6%) is observed over the next thermal cycle, mostly near the surface with the third time step causing negligible further displacements. Sharp changes in contrast, notably at specimen edges can lead to some numerical errors in DVC computations at these locations; this may be seen for example, in the negative in-plane displacements (Fig. 3a) at the specimen extremities of the final cycle (40 to 60 hours).

The out of plane displacements along the TGO (Fig. 3b) indicate an upward displacement of 1 – 2µm following the first exposure period which is in accordance with metallographic observations of TGO growth (Fig. 4). The displacement gradient following the first exposure period was estimated as 0.7% suggesting that the oxide growth is not uniformly normal and the bondcoat oxidation rate is higher at the exposed surface. As with the in-plane data, the final time step (40 to 60 hours) produced a negligible out-of-plane displacement due to the decrease in oxide growth rate in accordance with expected kinetics; the out-of-plane displacements for the second time step are not shown in Fig. 3b due to a lack of sufficient correlation of microstructural features adjacent to the TGO within the competition zone of the topcoat. Destructive cross-sections (Fig. 4) show an increase in inter-columnar separations at the base of the topcoat (Fig. 4a and 4b) due to bond-coat creep, and thickening of the TGO (Fig. 4c), which together may be the cause of the measured displacements. This change in the structure may also contribute to the lack of DVC correlation between the 40 hour and 60 hour exposures.

This study has demonstrated the capability of combined synchrotron X-ray computed micro-tomography and digital volume correlation in quantifying displacements within a thermal barrier coating system under pseudo in-situ cyclic exposure at 1200°C. It is proposed that displacement field measurements, obtained using the technique presented herein, may be combined in future with TBC failure prediction models that estimate TGO growth and bondcoat oxidation strain prediction and consequently validate TBC failure models.

[1]   Busso EP, Qian ZQ, Taylor MP, Evans HE. Acta Mater 2009;57:2349.
[2]   Heeg B, Tolpygo VK, Clarke DR. J Am Ceram Soc 2011;94:112.
[3]   Siddiqui SF, Knipe K, Manero AC, Meid C, Wischek J, Okasinski J, Almer J, Karlsson AM, Bartsch M, Raghavan S. Rev Sci Instrum 2013;84:1.
[4]   Diaz R, Jansz M, Mossaddad M, Raghavan S, Okasinski J, Almer J, Pelaez-Perez H, Imbrie PK. Appl Phys Lett 2012;100:1.
[5]   Manero II A, Sofronsky S, Knipe K, Meid C, Wischek J, Okasinski J, Almer J, Karlsson AM, Raghavan S, Bartsch M. JOM 2015:1.
[6]   Vassen R, Stuke A, Sto D, Ju F. J Therm Spray Technol 2009;18:181.
[7]   Evans HE. Surf Coatings Technol 2011;206:1512.
[8]   Ahmadian S, Browning A, Jordan EH. Scr Mater 2015;97:13.
[9]   Maurel V, Helfen L, N'Guyen F, Köster A, Di Michiel M, Baumbach T, Morgeneyer TF. Scr Mater 2012;66:471.

[10] Bay BK, Smith TS, Fyhrie DP, Saad M. Exp Mech 1999;39:217.
[11] Mostafavi M, Baimpas N, Tarleton E, Atwood RC, McDonald SA, Korsunsky AM, Marrow TJ. Acta Mater 2013;61:6276.
[12] Germaneau A, Doumalin P, Dupré JC. NDT E Int 2008;41:407.
[13] Mostafavi M, Collins DM, Cai B, Bradley R, Atwood RC, Reinhard C, Jiang X, Gelano M, Lee PD, Marrow TJ. Acta Mater 2015;82:468.
[14] Eberl C, Gianola DS, Wang X, He MY, Evans AG, Hemker KJ. Acta Mater 2011;59:3612.
[15] Rickerby DS, Bell SR, Wing RG. Article Including Thermal Barrier Coated Superalloy Substrate. US5981091, 1999.
[16] Drakopoulos M, Connolley T, Reinhard C, Atwood R, Magdysyuk O, Vo N, Hart M, Connor L, Humphreys B, Howell G, Davies S, Hill T, Wilkin G, Pedersen U, Foster A, De Maio N, Basham M, Yuan F, Wanelik K. J Synchrotron Radiat 2015;22:828.
[17] Titarenko S, Withers PJ, Yagola A. Appl Math Lett 2010;23:1489.
[18] Gerward L, Guilbert N, Jensen KB, Levring H. Radiat Phys Chem 2004;71:653.
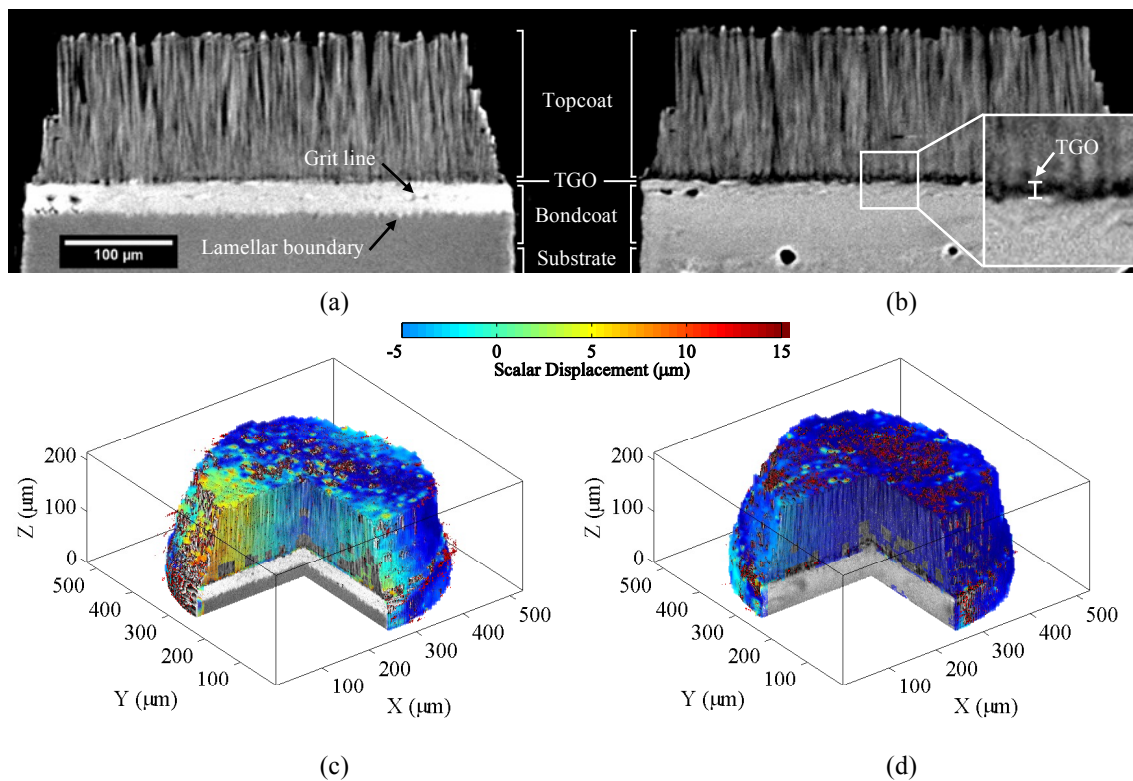
(a)

(b)

(c)

(d)

Figure 1 – Reconstructed sections of TBC samples in (a) as-received condition and (b) following 40 hours at 1200°C (note the X-ray attenuation of the TGO is similar to air; both appear dark compared to the substrate); and three-dimensional DVC computed scalar displacement field showing the total magnitude of 3D displacements for (c) time-steps one and two (i.e., as-received and twenty hours) overlaid onto as-received reconstruction and (d) 20 hours and 40 hours overlaid onto the reconstruction after 20 hours at 1200°C. Please note that 'scalar displacements' were calculated from magnitudes of 3-D Cartesian point displacements of combinatorial X-ray attenuation data.
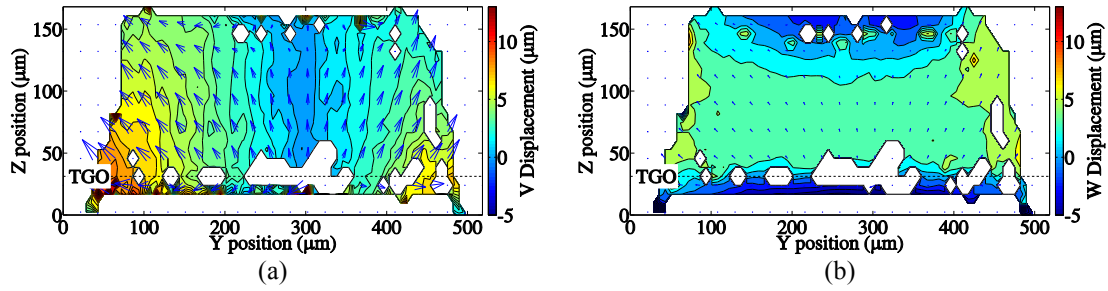
Figure 2 – A 2-D DVC scalar displacement vector field for a central Y-Z plane after 20 hours at 1200°C, contour map showing scalar displacement components (a) in the plane of the TGO and (b) normal to the plane of the TGO. Please note that 'scalar displacements' were calculated from magnitudes of 3-D Cartesian point displacements of combinatorial X-ray attenuation data.
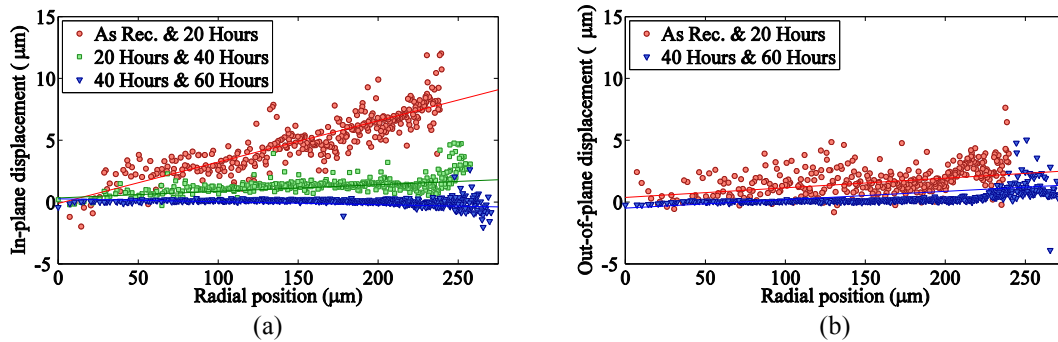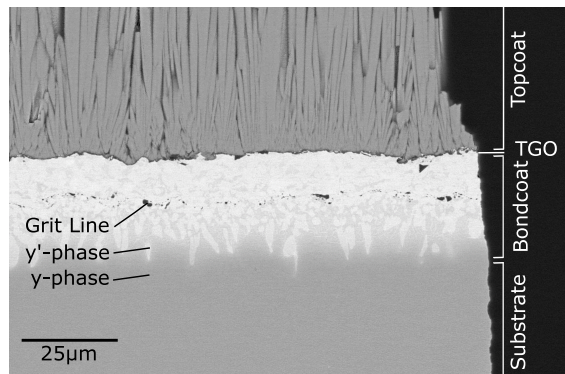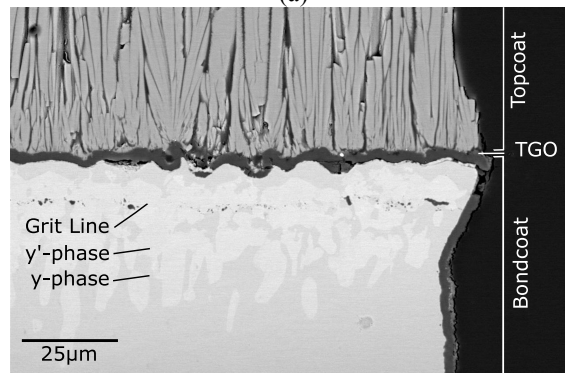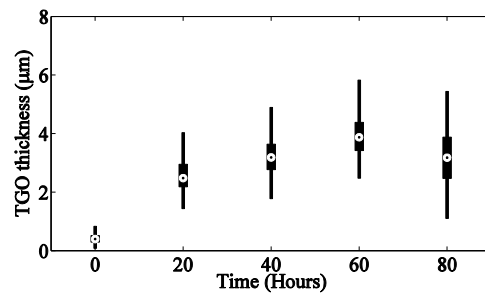

Figure 3 – Displacement profiles extracted from the DVC data in the specimen centre showing (a) normal displacements through the TGO, (b) in-plane displacements through the TGO about the specimen cylindrical axis.

(a)

(b)

(c)

Figure 4 – Destructive cross-sections of samples similar to those examined via tomography and digital volume correlation in this work (a) in the as-received state, (b) following 20 hours at 1200°C where δ indicates the outward displacement relative to the original substrate boundary and (c) TGO thickness measurements. Central point indicates median TGO thickness while thick bars indicate 25th and 75th quartiles and thin bars indicate range of values for non-outlier thicknesses.